J Mater Sci: Mater Electron (2017) 28:8397–8404
DOI 10.1007/s10854-017-6557-7

Dielectric and piezoelectric properties of $0.99Bi_{0.5}(Na_{0.82}K_{0.18})_{0.5}Ti_{(1-x)}Nb_xO_3$-$0.01NaSbO_3$ ceramics

Amir Ullah[1,2] · Aman Ullah[3] · M. Javid Iqbal[4] · M. Naeem Khalid[1] · Asim Ali[1] · Aurang Zeb[1] · Tahirzeb Khan[5] · Ill Won Kim[2]

Received: 8 December 2016 / Accepted: 7 February 2017 / Published online: 24 February 2017

Abstract Lead-free piezoelectric ceramic compositions in the system: $0.99Bi_{0.5}(Na_{0.82}K_{0.18})_{0.5}Ti_{(1-x)}Nb_xO_3$-$0.01NaSbO_3$ ($x=0$–0.04) were prepared by solid state reaction method. Room temperature (RT) X-ray diffraction confirmed that the crystal structure was changed from rhombohedral at $x=0$ to pseudocubic symmetry with the increase of Nb-content. Polarization versus electric field (P–E) hysteresis loops displayed a decline in remnant polarization (P_r) and coercive field (E_c) The piezoelectric charge coefficient (d_{33}) measured was ~135 pC/N at $x=0$ decreased to ~7 pC/N for the Nb-rich ceramics. A high field-induced normalized strain coefficient ($S_{max}/E_{max}=d^*_{33}$) of 610 pm/V was observed for the composition with 3 mol% Nb content.

1 Introduction

Lead-based ceramics, such as lead zirconate titanate ($PbZr_{1-x}Ti_xO_3$, PZT) have extra-ordinary electromechanical properties and are, therefore, widely used in sensors, actuators and transducers [1]. However, environmental concerns over the use of lead (Pb) diverted ceramicist's attention towards the development of Pb-free piezoelectric ceramics, especially; Bi containing perovskite compounds [1–4]. Among these lead-free, $(Bi_{0.5}Na_{0.5})TiO_3$ (BNT)-based ceramics near the morphotropic phase boundary (MPB) are considered as possible alternatives for Pb-based ceramics [5]. The solid solution of $(Bi_{0.5}Na_{0.5})TiO_3$ (BNT) and $(Bi_{0.5}K_{0.5})TiO_3$ (BKT) at MPB exhibited a number of characteristics similar to $PbZr_{1-x}Ti_xO_3$ ceramics. To improve the electric field induced strain of these ceramics for actuator applications, various materials were doped in these Bi-based complex perovskites and have been investigated [6–8]. The $Bi_{0.5}Na_{0.5}TiO_3$-$Bi_{0.5}K_{0.5}TiO_3$ (BNKT) system has been reported to exhibit high strain and ferroelectric properties, when Na^+ is partially substituted for K^+ on the A-site of BNKT ceramics [9–12].

Ferroelectric crystals have asymmetric or polar structures and their constituent ions undergo asymmetric displacement when subjected to external electric field, leading to a small change in crystal dimensions proportional to the applied electric field [13–15]. This change is generally very small and thus limits its potential applications. $Bi_{0.5}(Na,K)_{0.5}TiO_3$ compounds doped on the A- and/or B-Site can be considered behave like ABO_3-type perovskites with Bi^{3+}, K^+, and Na^+ localized at the A-Site and Ti^{4+} at the B-site. In spite, the observed similarities in structure and properties, the piezoelectric properties of BNT–BKT solid solutions still lack the commercialization potential and require improvements. In order to further improve the piezoelectric properties, BNT–BKT solid solution was modified either by doping or making another solid solution with other perovskite-structured materials [16–19].

The incorporation of $LiSbO_3$ or $AgSbO_3$ into $Na_{0.5}K_{0.5}NbO_3$ solid solution, and $NaNbO_3$ or $LiNbO_3$

✉ Amir Ullah
aamiru8@gmail.com

1 Department of Physics, Islamia College, Peshawar 25120, Khyber Pakhtunkhwa, Pakistan

2 Department of Physics and EHSRC, University of Ulsan, Ulsan 680-749, Republic of Korea

3 Department of Physics, University of Science and Technology, Bannu, Khyber Pakhtunkhwa, Pakistan

4 Department of Physics, University of Peshawar, Peshawar, Khyber Pakhtunkhwa, Pakistan

5 Department of Physics, Abdul Wali Khan University, Mardan 23200, Khyber Pakhtunkhwa, Pakistan

into BNT–BKT ceramics has been reported to enhance the piezoelectric coefficient (d_{33}) and electromechanical coupling factor (k_p) [20–22]. Rong and Yuan [23] studied the $LiSbO_3$-doped $Bi_{0.5}(Na_{0.82}K_{0.18})TiO_3$ ceramics system and reported an improvement in its piezoelectric and dielectric properties. Zuo et al., investigated the effect of $NaSbO_3$ on piezoelectric properties of BNKT; $(1-x)Bi_{0.5}(Na_{0.82}K_{0.18})_{0.5}TiO_3$-$xNaSbO_3$ (BNKT-NB) and reported an enhanced piezoelectric coefficient ($d_{33} \sim 160$ pC/N) and electromechanical coupling factor ($k_p \sim 0.333$) at $x = 0.01$ compared to that of pure BNKT ceramics [24]. Furthermore, it has been reported that $NaSbO_3$ can greatly affect bulk density, grain size, poling state and ferroelectricity when incorporated to BNT-based ceramics [24]. As Sb^{5+} ion has large electronegativity and relatively smaller ionic size than that of Ti^{4+}, so Sb^{5+} cation has more off centering than that of Ti^{4+} cation. BNT is A-site piezoelectric active and N^{a+} enters into A-site of BNT ceramics, causing the improvement of piezoelectric properties. However, the electric field induced strain and ferroelectric properties of BNKT-NB system was not studied and discussed.

Therefore, keeping in view the importance of electric field induced strain for actuator applications, the system $0.99Bi_{0.5}(Na_{0.82}K_{0.18})_{0.5}TiO_3$-$0.01NaSbO_3$ was selected as a base material due to its promising piezoelectric properties. The effect of Nb concentration on the phase, microstructure, dielectric, ferroelectric and field-induced strain of $0.99Bi_{0.5}(Na_{0.82}K_{0.18})_{0.5}Ti_{(1-x)}Nb_xO_3$-$0.01NaSbO_3$ (BNKTN-NS) ($x = 0$–0.04) ceramics was investigated in detail.

2 Experimental

Lead-free ceramics in $0.99Bi_{0.5}(Na_{0.82}K_{0.18})_{0.5}Ti_{(1-x)}Nb_xO_3$-$0.01NaSbO_3$ ($x = 0$–0.04) system were prepared by a conventional solid state reaction method. Sb_2O_5 (99.9%) and Nb_2O_5 (99.9% Cerac Specialty In-organics, USA) and Bi_2O_3, Na_2CO_3, K_2CO_3, TiO_2 (99.9% High Purity Chemicals, Japan) were used as initial ingredients in the present study. Carbonates and oxides were dried at 100 °C for 24 h to remove moisture prior to batch preparation. The raw materials were weighed in stoichiometric ratios and ball milled for 24 h in disposable polyethylene mill jars, using ethanol as lubricant and Y-toughened zirconia balls as grinding media. The slurries were dried overnight at 90 °C, ground and then calcined at 850 °C for 2 h in closed alumina crucibles. The calcined powders were milled again to dissociate agglomerates and further reduce the particle size. After thoroughly mixing with an aqueous polyvinyl alcohol (PVA) solution, the powders were pressed into 10 mm diameter pellets at ~100 MPa. The pellets were heated at 500 °C to remove PVA and then sintered at 1170 °C for 2 h in closed alumina boats buried in the atmospheric powder to reduce the volatilization of the volatile substances. Structural and phase analysis of the sintered ceramics was investigated using X' Pert-PRO MRD, Philips, KBSI X-ray diffractometer. As-sintered samples were finely polished and thermally etched at 1050 °C for 30 min. Finally, a field-emission scanning electron microscope (FE-SEM, Hitachi.S-4200 & Japan) was used to investigate the microstructure of the sintered ceramics samples.

For electrical characterization, silver paste was printed on the whole pellet surfaces of both sides, followed by heating at 700 °C for 30 min. The temperature dependence of the dielectric properties was measured using an impedance analyzer (HP4192A). The piezoelectric constant, d_{33}, was measured using a piezo-d_{33} meter (ZJ-6B, China). The electric-field-induced strain was measured using a linear variable differential transducer (LVDT, Mitutoyo MCH-331 & M401).

3 Results and discussion

3.1 Phase and microstructure

Figure 1 shows the room temperature (RT) X-ray diffraction (XRD) patterns of BNKTN-NS ($x = 0$–0.04) ceramics samples. The XRD patterns revealed that the samples crystallized into single phase ceramics with perovskite structure. As shown in expanded XRD pattern in 2θ range 38°–48°, composition x = 0 displayed a rhombohedral symmetry apparent from the small shoulder of (111) peak and broadend (200) peak. So the un-doped BNKTN-NS ceramic composition could be indexed for rhombohedral, while for $x \geq 0.03$ could be indexed for pseudocubic symmetry. Moreover, the intensity was also found to increase with increasing Nb content.

Figure 2 exhibited the FE-SEM micrographs of BNKTN-NS ($x = 0$, 0.02, 0.03 and 0.04) ceramics. The microstructure of the $x = 0$ composition comprised irregular-shaped grains appearing diffused into one another, results larger grains. However, the average grain size gradually decreased from ~1.5 μm for the $x = 0$ composition to ~0.7 μm for the $x = 0.04$ composition which demonstrated that Nb incorporation suppressed grain growth. All the samples exhibited a reasonably dense microstructure with clear grains and grain boundaries. The densities of the samples were found to be slightly increased with an increase in Nb concentration as shown in Table 1. The optimal concentration of Nb for improving densification seems to be $x = 0.03$.

The formation of vacancy on the A-site may contribute to the improved densification based on enhanced mass

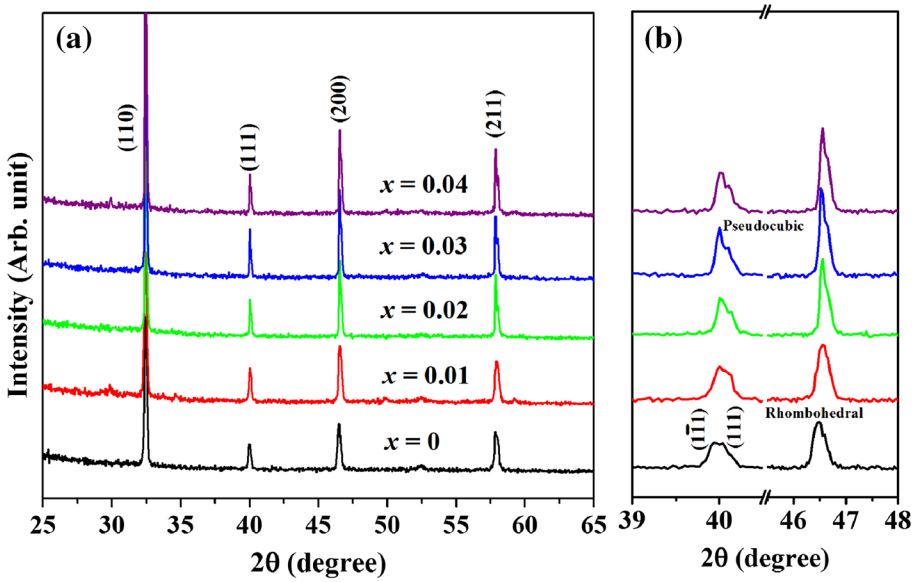

Fig. 1 X-ray diffractions patterns of BNKTN-NS ($x = 0$–0.04) ceramics in 2θ range of **a** 25°–65° and **b** 39°–48°

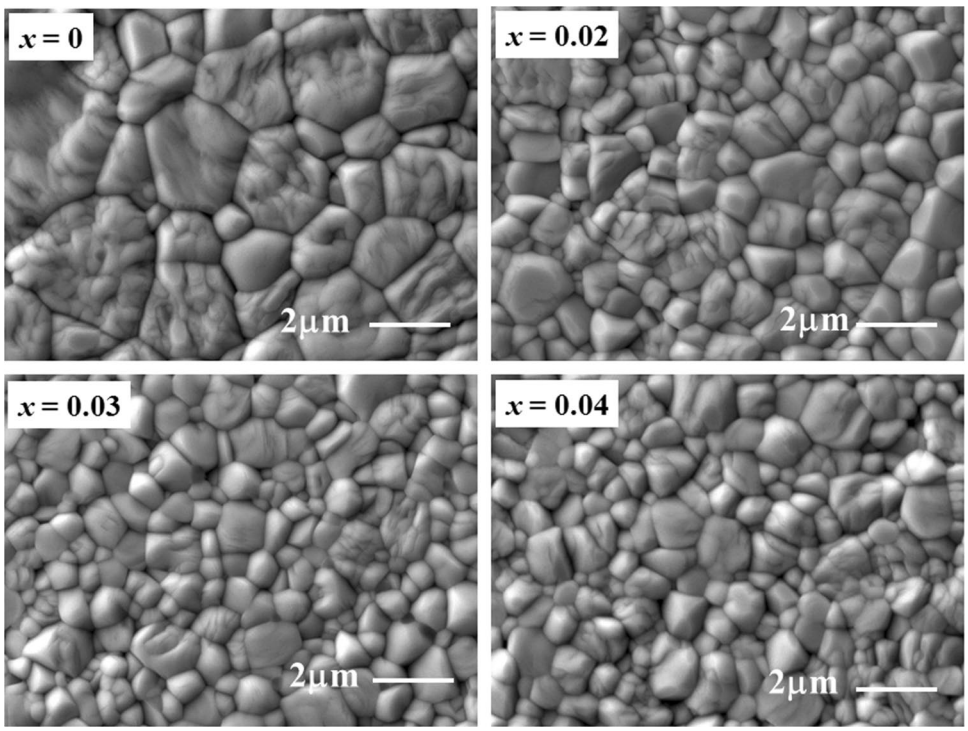

Fig. 2 Field-emission scanning electron microscopic images of BNKTN-NS ($x = 0$, 0.02, 0.03 and 0.04) ceramics

Table 1 Physical and electrical properties of BNKTN-NS ceramics sintered at 1170 °C

BNKTN-NS	Grain size (μm)	ρ (g/cm^3)	T_d (°C)	ε (RT)	tanδ (%)	E_c (kV/cm)	d_{33} (pC/N)	d^*_{33}(pm/V)
0	1.75	5.81	140	1371	6.0	41.3	135	213
0.01	0.86	5.86	105	1128	5.7	38.5	67	328
0.02	0.74	5.88	53	1636	5.5	17.4	46	404
0.03	0.66	5.90	45	1567	5.2	12.2	22	610
0.04	0.61	5.87	40	1550	5.3	9.0	07	347

transportation ability. In addition, the excessive Nb dispersed at the grain boundary tends to pin the boundary motion as described in [25].

3.2 Dielectric properties of BNKTN-NS ceramics

The relative permittivity or dielectric constant (ε_r) and loss tangent (tanδ) as a function of temperature of the ceramic system BNKTN-NS at selected frequencies 1, 10 and 100 kHz were plotted in Fig. 3. All the dielectric curves in ε_r displayed two peaks correspond to depolarization T_d and temperature of maximum relative permittivity T_m. For $x=0$ composition, T_d was observed at ~140 °C; however, with an increase in Nb ($x=0.04$), T_d decreased to ~RT.

The second dielectric anomaly corresponds to the temperature of maximum relative permittivity was observed at around $T_d \sim 265$ °C for all investigated samples. However, with increasing Nb content in the solid solution, both the anomalies (T_d and T_m) became relatively more flat, signifying the formation of relaxor phase. Patterson and Pham et al. reported similar behavior in BNKT based ceramics [26, 27]. Moreover, apart from the two characteristics temperature T_d and T_m another characteristic temperature where the frequency dispersion almost vanished (denoted as T_{DV}) was also noticed. It was observed that the frequency dispersion behavior increased with increasing Nb content and could be suggested the relaxor characteristics for BNKTN-NS ceramics.

At low temperatures A-site cations has displacement which are antiparallel to those of B-site cations within each individual nanodomain and this incomplete cancellation of the dipole moments will generate a net polarization effect [28]. Hence, the dynamic fluctuation of the weakly polar nanodomains leads to the relaxor behavior.

The loss tangent of BNKTN-NS ceramics was observed to be very low at temperatures below 400 °C and almost constant for all the compositions with negligible dispersion; however, it increased at temperatures above 400 °C.

Figure 4 shows the plots of $\log(1/\varepsilon - 1/\varepsilon_m)$ versus $\log(T-T_m)$ at 1 kHz for the BNKTN-NS ceramics (0, 0.01, 0.03 and 0.04). The diffuse characteristics of ferroelectric to paraelectric phase transition could be ascribed to the deviation from typical Curie–Weiss law to modified Curie–Weiss relationship. The degree of disorder or diffusivity (γ) in the ceramics were measured by using the empirical relation $\log(1/\varepsilon - 1/\varepsilon_m) = \log K + \gamma \log(T-T_m)$ [29]. In this relation ε_m is known as the maximum value of dielectric constant at T_m and K is an arbitrary constant. The values of γ for the BNKTN-NS ceramics at 1 kHz were estimated from the slope of the curves on the plot of $\log(1/\varepsilon - 1/\varepsilon_m)$ versus $\log(T-T_m)$. The estimated diffusivity values (γ) were found to be between 1 (obeying the Curie–Weiss law) and 2 (for a completely disordered system).

The obtained values of $\gamma = 1.76$, 1.85, 1.80 and 1.87 at $x=0$, 0.01, 0.03 and 0.04, respectively, indicating a deviation from Curie–Weiss behavior ($\gamma=1$), which suggests the occurrence of disordering in the BNKTN-NS system [30].

3.3 Ferroelectric properties of BNKTN-NS ceramics

Figure 5 displays the RT polarization–electric field hysteresis loops (P–E) for BNKTN-NS ceramics at an

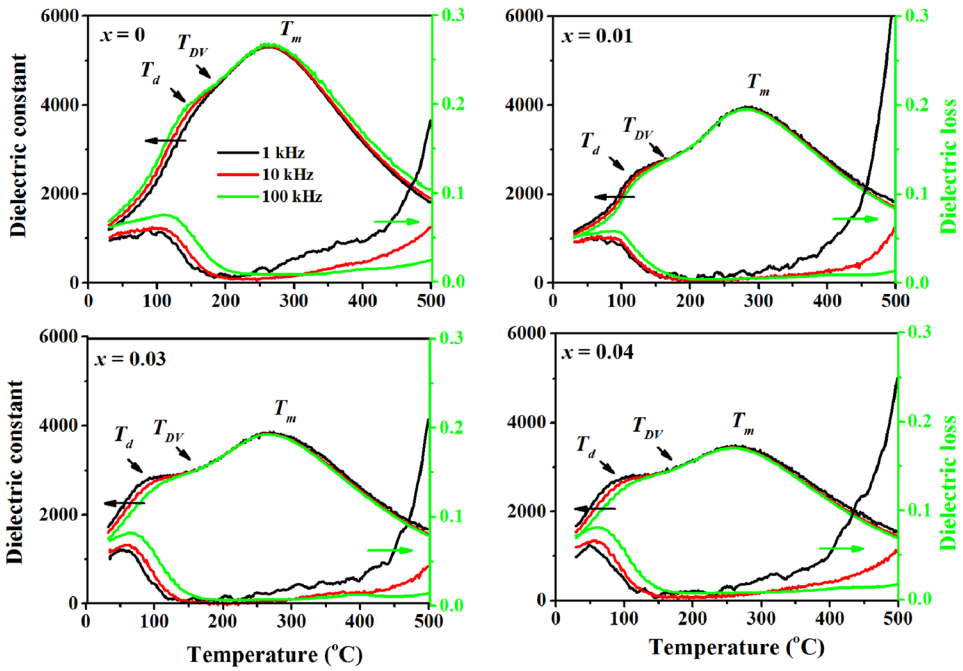

Fig. 3 Temperature dependent dielectric constant and loss of poled samples of BNKTN-NS ceramics at 1, 10 and 100 kHz

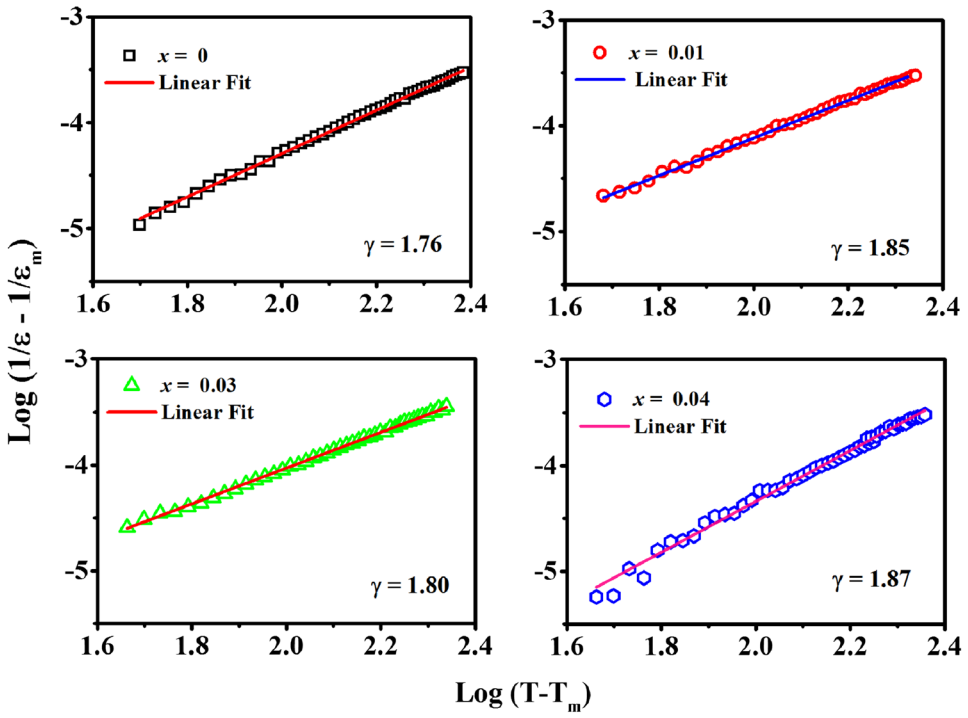

Fig. 4 The plots of $\log(1/\varepsilon - 1/\varepsilon_m)$ versus $\log(T - T_m)$ (γ-value) at 1 kHz for the BNKTN-NS (0, 0.01, 0.03 and 0.04) ceramics

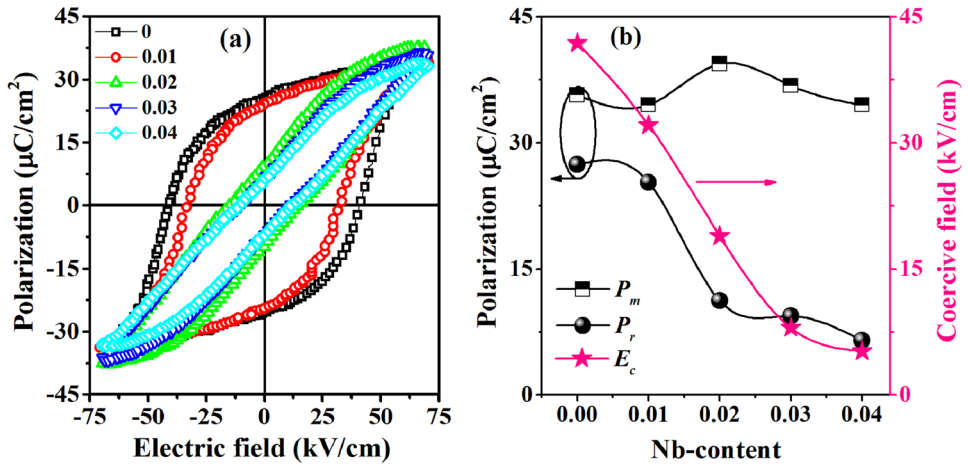

Fig. 5 **a** Polarization electric field (P–E) hysteresis loops and **b** the effect of Nb- contents on the ferroelectric properties of BNKTN-NS ($x = 0$–0.04) ceramics

applied electric field of 70 kV/cm. A square shaped *P–E* loop, typical of ferroelectric materials consistent with those of BNT [31, 32] based ceramics was observed for $x = 0$ composition. The composition at $x = 0$ exhibited a high remnant polarization (P_r) of 30 μC/cm^2, maximum polarization (P_m) of 40 μC/cm^2 and a coercive field (E_c) of 40 kV/cm. However, with the increase of Nb concentration to $x = 0.01$, P_r was observed to decrease slightly. The incorporation of Nb concentration beyond $x = 0.01$, transformed the *P–E* loops from the typical ferroelectric to slightly pinched-shaped along with a decline in P_r and E_c. Moreover, at high Nb content, the *P–E* loops became slim with smaller P_r and E_c and exhibited almost a relaxor-like behavior which is consistent to that observed in the reported literature [33].

The ceramic sample $x = 0.030$, which displayed a high strain value was studied with respect to temperature. At temperature 90 °C, the hysteresis was found to pinched shape and was in agreement with results of *S–E* loops and dielectric constant of this material which was clarified the transition from typical FE to relaxor state at around T_d. Moreover, the *P–E* loop maintain P_m and P_r with increasing temperature and however, the coercive field E_c was decreased.

3.4 Electric field-induced-strain response of BNKTN-NS ceramics

Figure 6 exhibited the influence of Nb doping on the bipolar electric field induced strain of BNKTN-NS ceramics. The composition with $x=0$, demonstrated a ferroelectric (FE) order typical butterfly-shaped strain hysteresis loops with a negative strain (S_n) 0.09% and maximum strain (S_m) 0.15% strain during bipolar cycles. However, when the Nb concentration was increased to $x=0.04$, the strain loops was disrupted and the behavior can be ascribed to transition from FE to a relaxor or non-polar state. The bipolar strain was found to increase with increase in Nb content up to $x=0.03$ and then decreased. The maximum strain S_m of 0.43% with almost negligible negative strain for $x=0.03$ was observed at applied electric field of 70 kV/cm. The remnant polarization and coercive field were decreased when the Nb doping level was increased and also in agreement of the polarization study of this material where the *P–E* loop become slim for doping Nb concentration. The results obtained were found to be in consistent as observed by other researchers for BNT based systems [4, 14–16].

Figure 7 displayed the RT unipolar strain of BNKTN-NS ($x=0$–0.04) ceramics at an electric field of 70 kV/cm. For the compositions with $x>0.01$, the observed change in the shape of the electric field induced strain (i.e. *S–E* loop) at a threshold electric field, demonstrated a field induced polar to non-polar phase transition, consistent with previous studies [31–34]. The maximum unipolar strain of 0.43% at an applied field of 70 kV/cm was achieved for the BNKTN-NS ceramics at $x=0.03$. Furthermore, the unipolar strain curves did not exhibit negative strain for the $x=0.01$ composition and were highly symmetric, describing the typical field induced co-existing polar and

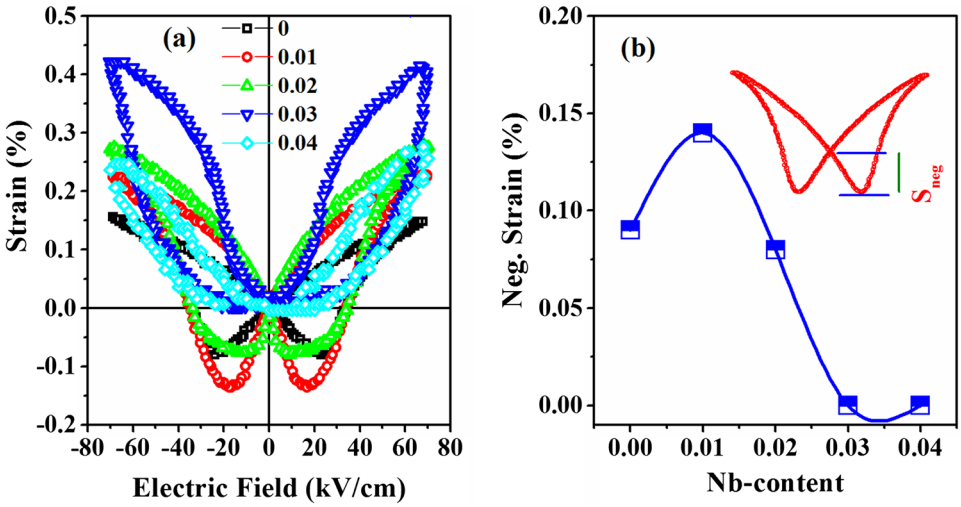

Fig. 6 **a** Room temperature bipolar strain at an applied electric field of 70 kV/cm and **b** corresponding negative strain values of BNKTN-NS ($x=0$–0.04) ceramics

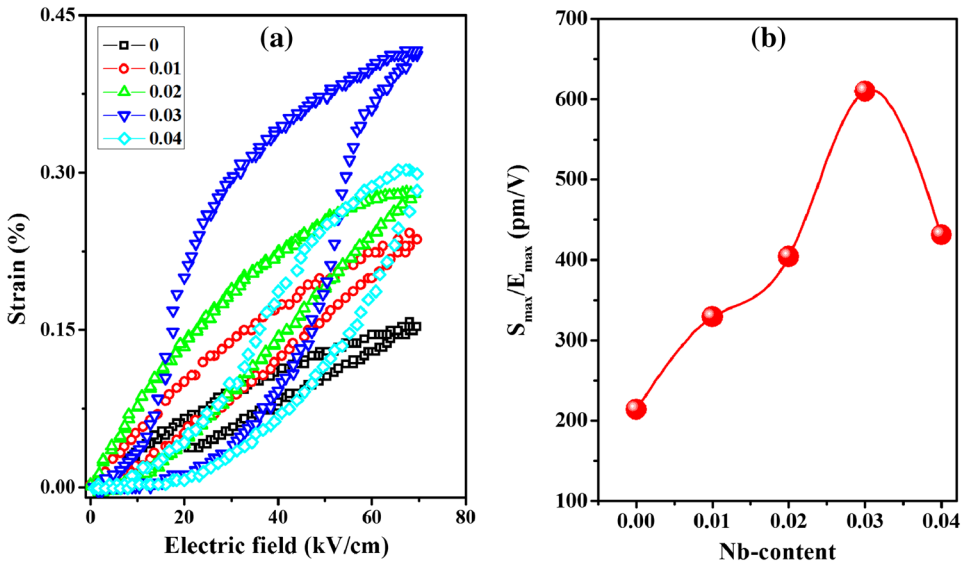

Fig. 7 **a** Room temperature unipolar strain curves at an electric field of 70 kV/cm and **b** corresponding S_{max}/E_{max} values of BNKTN-NS ($x=0$–0.04) ceramics

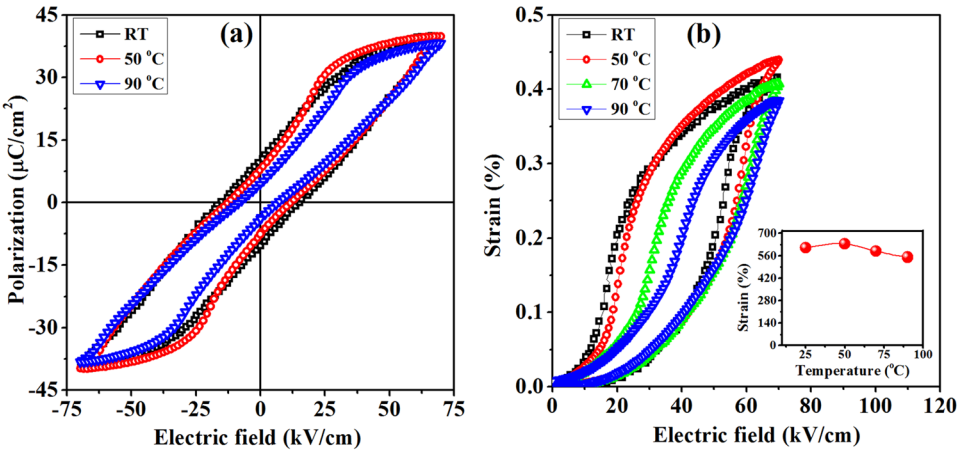

Fig. 8 **a** Temperature dependent polarization hysteresis loops and **b** temperature dependent unipolar strain curves for BNKTN-NS with Nb = 0.03

non-polar ferroelectric orders. The polarization behavior also supported the obtained strain trend as evidenced by the significant construction of *P–E* loop at this critical composition (i.e. $x = 0.01$). Moreover, the disruption of the long range ferroelectric order started and became more pronounced due to the incorporation of Nb ratios. This resulted in a drastic decrease of piezoelectric properties ($d_{33} = 7$ pC/N) and enhancement of the converse piezoelectric effect with a large normalized strain($S_{max}/E_{max} = d^*_{33} = 6$ 10 pm/V) (Fig. 7).

The overall picture evident from the dielectric, ferroelectric and strain data (Figs. 3, 5, 6, 7), demonstrated that T_d, P_r, E_c and static d_{33} decreased and the normalized or dynamic strain gradually increased to a peak value of 610 pm/V with an increase in Nb content up to $x = 0.03$, and then decreased upon further increase in x (Table 1). These results confirmed the transition from a polar to a relaxor state. Moreover, the observed increase in strain may be due to ferroelectric domain switching and field induced ferroelectric to relaxor phase transition or both [35]. Thus, the composition with $x = 0.03$ showed a dominant relaxor behavior with very small remnant polarization and slim and pinched type *P–E* loops.

Figure 8 displayed the temperature dependent unipolar *S–E* curves for BNKTN-NS with Nb = 0.03. The ceramic exhibited the same behavior as presented in the temperature dependent *P–E* loop. Strain was found to increase to its maximum value of 635 pm/V when temperature was increased to 50 °C and however, then decreased with further increased in temperature. The S_{max}/E_{max} reached to the maximum of 610 and 557 pm/V at RT and 90 °C, respectively which exhibited quite weak temperature-dependent behavior. The large strain jump at around T_d and that can be attributed to the non-180 polarization switching and depolarization at T_d [33] Therefore, the temperature stable property of this system would be quite favorable for high-temperature application.

4 Conclusions

Single phase and dense ceramics were fabricated in the system: BNKTN-NS (x = 0–0.04). RT XRD revealed a phase transition from rhombohedral to pseudocubic symmetry with increasing in Nb concentration. Furthermore, with increasing Nb content, both the anomalies (T_d and T_m) on the relative permittivity and loss tangent versus temperature plots flattened, suggesting a composition-induced ferroelectric to relaxor or non-polar transition. At high Nb contents, the *P–E* loops became slim and transformed to deformed or pinched shaped loops along with a drastic decline in P_r and E_c exhibited a relaxor-like behavior. A high normalized strain (S_{max}/E_{max}) of 610 pm/V was obtained at 3 mol% Nb content under an applied field of 70 kV/cm. The disruption of the long range ferroelectric order began and became more pronounced with increasing Nb concentration, resulting in a drastic decrease in d_{33} to 7 pC/N, demonstrating it to be a potential candidate material for piezoelectric applications.

Acknowledgements This work was supported by Basic Science Research program through the National Research Foundation of Korea (NRF) funded by the Ministry of Education (2014R1A1A4A01004404).

References

1. A. Zeb, S.J. Milne, J. Am. Ceram. Soc. **97**(8), 2413 (2014)
2. T.R. Shrout, S.J. Zhang, J. Electroceram. **19**, 113 (2007)
3. J. Hao, B. Shen, J. Zhai, C. Liu, X. Li, X. Gao, J. App. Phys. **113**, 114106 (2013)
4. A. Zeb, D.A. Hall, S.J. Milne, J. Mater. Sci. **26**, 9516–9521 (2015)
5. A. Sasaki, T. Chiba, Y. Mamiya, E. Otsuki, Jpn. J. Appl. Phys **38**, 5564 (1999)

6. A. Ullah, C.W. Ahn, A. Ullah, I.W. Kim, Appl. Phys. Lett. **103**, 022906 (2013)
7. V.Q. Nguyen, H.S. Han, K.J. Kim, D.D. Dang, K.K. Ahn, J.S. Lee, J. Alloy. Compd. **511**, 237 (2012)
8. F. Wang, M. Xu, Y. Tang, T. Wang, W. Shi, C.M. Leung, J. Am. Ceram. Soc. **95**, 1955 (2012)
9. K. Yoshii, Y. Hiruma, H. Nagata, T. Takenaka, Jpn. J. Appl. Phys. **45**, 4493 (2006)
10. Z. Yang, B. Liu, L. Wei, Y. Hou, Mater. Res. Bull. **43**, 81 (2008)
11. M. Izumi, K. Yamamoto, M. Suzuki, Y. Noguchi, M. Miyayama, Appl. Phys. Lett. **93**, 242903 (2008)
12. S. Zhao, G. Li, A. Ding, T. Wang, Q. Yin, J. Phys. D **39**, 2277–2281 (2006)
13. N.D. Quan, L.H. Bac, D.V. Thiet, V.N. Hung, D.D. Dung, Adv. Mater. Sci. Eng. 2014, 365391 (2014)
14. M.E. Lines, A.M. Glass, *Principles and applications for ferroelectrics and related materials*. (Oxford University Press, Oxford, 1979)
15. K. Uchino, *Piezoelectric actuators and ultrasonic motors*. (Kluwer Academic Publishers, Boston, 1996)
16. A. Ullah, A. Ullah, I.W. Kim, D.S. Lee, S.J. Jeong, C.W. Ahn, J. Am. Ceram. Soc. **97**(8), 2471 (2014)
17. N.B. Do, H.B. Lee, C.H. Yoon, J.K. Kang, J.S. Lee, Trans. Electr. Electron. Mater. **12**, 64 (2011)
18. A. Singh, R. Chatterjee, J. Appl. Phys. **109**, 024105 (2011)
19. S.T. Zhang, A.B. Kounga, E. Aulbach, Appl. Phys. Lett. **91**, 112906 (2007)
20. D.M. Lin, K.W. Kwok, H.L. Chan, J. Appl. Phys. **10**, 074111 (2007)
21. Y.M. Li, W. Chen, Q. Xu, J. Zhou, H.J. Sun, M.S. Liao, J. Electroceram. **14**, 53 (2005)
22. C.R. Zhou, X.Y. Liu, W.Z. Li, C.L. Yuan, J. Phys. Chem. Solids **70**, 541 (2009)
23. Z.C. Rong, C.L. Yuan, Bull. Mater. Sci. **34**, 933 (2011)
24. Q. Zhou, C. Zhou, W. Li, J. Cheng, H. Wang, C. Yuan, J. Phys. Chem. Sol. **72**, 909 (2011)
25. R. Zuo, H. Wang, B. Ma, L. Li, J. Mater. Sci. **20**, 1140 (2009)
26. E.A. Patterson, D.P. Cann, J. Pokorny, I.M. Reaney, J. Appl. Phys. **111**, 094105 (2012)
27. K.N. Pham, H.B. Lee, H.S. Han, J.K. King, J.S. Lee, A. Ullah, C.W. Ahn, I.W. Kim, J. Korean Phys. Soc. **60**, 20 (2012)
28. X.L. Tan, C. Ma, J. Frederick, S. Beckman, K.G. Webber, J. Am. Ceram. Soc. **94**, 4091 (2011)
29. S.M. Pilgrim, A.E. Sutherland, S.R. Winzer, J. Am. Ceram. Soc. **73**, 3122 (1990)
30. W.P. Cao, W.L. Li, Y. Feng, D. Xu, W. Wang, Y.F. Hou, T.D. Zhang, W.D. Fei, J. Phys. Chem. Solid **78**, 41 (2015)
31. A. Ullah, M. Alam, A. Ullah, C.W. Ahn, J.S. Lee, S. Cho, I.W. Kim, RSC Adv. **6**, 63915 (2016)
32. R. Cheng, Z. Xu, R. Chu, J. Hao, J.D.G. Li, RSC Adv. **5**, 41646 (2015)
33. P.Y. Chen, C.S. Chen, C.S. Tu, T.L. Chang, J. Eur. Ceram. Soc. **34**, 4223 (2014)
34. T.H. Dinh, M.R. Bafandeh, J.K. Kang, C.H. Hong, W. Jo, J.S. Lee, Ceram. Inter. **41**, 458 (2015)
35. S.T. Zhang, B. Yang, W. Cao, Acta. Mater. **60**, 469 (2012)